Supported by tetfund TERTIARY EDUCATION TRUST FUND

Dissipative Williamson-Casson Fluids Flow Over a Nonlinearly Stretching Sheet with Generalized Fourier's law and Soret Phenomenon: A Comparative Study

[1]Momoh, H.O., [2]Olatoye, A.O., [3*]Akolade, M.T., [4]Olabode, J.O., [5]Oyekunle, T.L., [6]Zhiri, A.B.

[1]Department of Mathematics and Statistics, Federal Polytechnic Nasarawa, Nasarawa State, Nigeria.
[2, 3, 4,5]Department of Mathematics, University of Ilorin, Ilorin, Nigeria.
[6]Department of Mathematics, Federal University of Technology, Minna, Nigeria.
*Corresponding Author: akolademojeed@yahoo.com

Received: March 20, 2022 **Accepted:** June 18, 2022

Abstract: The present comparative investigation unfolds the impacts of the soret mechanism, and generalized Fourier's law among other flow parameters on non-Newtonian fluids flow over a nonlinear stretching surface. The compared two non-Newtonian fluids herein include Williamson and Casson fluids, with the imposition of the magnetic field, inclination angle, radiation, soret, dissipation, Joule heat, and the assumption of the non-Fourier's concept. We utilized the appropriate similarity variables on the controlling flow PDEs models to obtain the required ODEs equations. The resulting ODEs systems are then solved numerically via the implementation of the collocation method with legendary polynomial as the basis function. In a limiting case, the model is in line with the earlier studies. The results herein identified that the Casson fluid possesses higher material conductivity than the Williamson fluid. The soret mechanism elevates the fluids flows, energy distributions, and fluid concentration significantly. Moreover, material with higher relaxation time signifies a lesser energy and velocity disposition throughout the entire medium. Other invaluable results are presented in the respective tables and graphs.

Keywords: Cattaneo-Christov, Casson fluid, Williamson Fluid, Soret phenomenon, Nonlinear Convection.

Introduction

Fluids like; water, blood, honey, mayonnaise, toothpaste, gels, ketchup, and consolidated milk are grouped into Newtonian and non-Newtonian classifications. With no gain saying, this fluid possesses different chemical and physical properties, thus making it difficult to represent these fluids with a single rheological model. Amid their usage, importance, and applications to engineers, scientists, and biomedical systems, this study finds it necessary to investigate numerically the comparative study of Williamson-Casson fluid flow over a nonlinearly stretching sheet with generalized Fourier's law and soret mechanism.

To this, authors like; Sarkar *et al* (2019) had enumerated the impact of magnetization, radiation, and chemical reaction over an inclined cylindrical plane. The simulation was conducted with the compact visualized FORTRAN algorithm, they deduced that heat and mass transfer distribution of Williamson fluid is lower in contrast to the Casson fluid. With dual heat flux over a heated stretchy sheet, Sivanandam and Eswaramoorthi (2019) examined the second law analysis of Casson-Williamson fluid, thus identifying that rise in Casson and Williamson numbers declined the impact of entropy generation rate. Investigation of cross-diffusion effect on Casson-Willamson is carried out by Bhuvaneswari *et al.* (2019), the study considered chemical reaction and radiation effect over a stretching sheet and highlighted the aggregation of concentration profile as Doufor number is enhanced. The stagnation point flow of Casson-Willamson fluid past an extended cylinder by Kumar *et al.* (2019) discusses the impact of a new heat flux model. The study employed the fourth order Runge-Kutta-based shooting system, and conclude that curvature parameter and thermal stratification tend to increase both energy and momentum field significantly. Recently Akolade and Tijani (2021) employed the spectral quasi-linearization method (SQLM) in the solution of the comparative examination of Casson-Willamson fluid in three-dimensional space. The study enumerated that lesser diffusion enhancement is observed in the case of Casson fluid compared to the Williamson fluid, to mention but a few out of the numerous studies.

To predict the warmth transfer across the flow vicinity correctly, for great utility in biomedical, engineering, cooling, and drug industries, Cattaneo (1948) opined that Fourier's law (1822) contradicts the concept of reality; therefore proposed a modified heat flux model which can address the relaxation time enhancement. This change become advanced by Christov (2009), thus named the model as Cattaneo-Christov. Eversince, several investigation of this concenpt on fluid rheology and geometrical surface have been recordrd. The contradiction surrounding Fourier's law of heat conduction and the idea of relativity was highlighted by Marin (2011). Akolade *et al.* (2021a) carried out the study of soret-Dufour with the implementation of the modified model on Casson fluid. Investigation of the modified flux model over a stretching surface with variable thickness was studied by Hayat *et al.* (2015). The analysis was conducted under the assumption of Maxwell fluid, they concluded that energy distribution is higher in the case of Fourier's law than in the modified heat flux model. Over a stretched cylinder filled with dust phase, Graphene, and silver nanoparticles, Upadhya *et al.* (2018) presented the modified Fourier heat flux on MHD flow over stretched cylinder filled with dust, Graphene, and silver nanoparticles. Their results signified that enhancement in thermal relaxation promotes energy profiles in both fluid and dust phase. Examination in porous stretching/shrinking sheet through a three-dimensional system is presented by Vishalakshi *et al* (2022), the investigation considered both heat and mass modified fluid.

The flow of non-Newtonian fluids over a nonlinearly stretching sheet had received great attention owing to its rich applicability in manufacturing industries, and engineering. Typical examples of boundary layer flow over a nonlinearly stretching sheet occur in areas like the production of glass fiber, coolant, etc (Devi and Prakash, 2016). Recent literature on this concept include the work of Oke *et al*. (2021), Idowu *et al*. (2021), Olabode *et al* (2021), and many others. This current comparative examination of soret mechanism, generalized Fourier's law, nonlinear convection, and variable electrical conductivity over a nonlinearly stretching sheet is believed far-fetched in the literature to authous best knowledge, hence, the study.

Model Formulation

Under the condition of the generalized heat flux model, this comparative study of two-dimensional flow Williamson-Casson fluid is assumed to be steady and incompressible on an inclined surface. Abolishing the regular assumption of Boussinesq approximation, the quadratic solution and thermal

convection are enumerated. Alongside the dissipation effect, the velocity slip and temperature jump impact is also considered. With applied MHD $B(x) = B_0 x^{\frac{m-1}{2}} \ (m \neq 1)$, and $U_0 = d_0 x^m$ being the stretching characteristics, and $h_i = d_0 x^{1-m}$ the material time relaxation rate, In Figure 1, displayed the induced along $x-axis$ and $y-axis$ perpendicular to it.

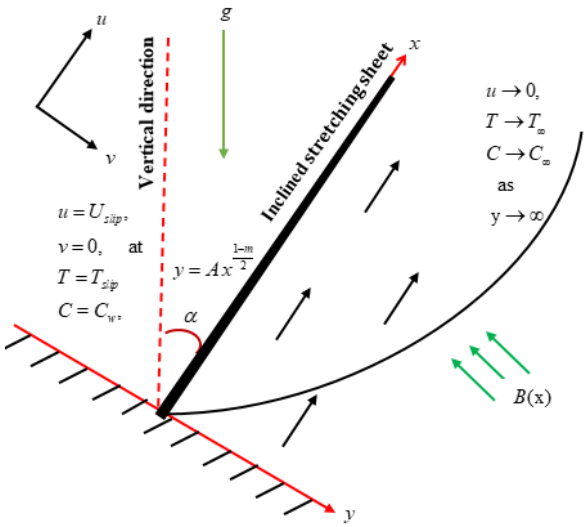

Figure 1: Flow model configuration.

Introducing the Rosseland approximation heat flux defined by (see Akolade et al. 2021b, Akolade and Tijani 2021):

$$q_r = -\frac{4\sigma^t}{3k_t}\frac{\partial T^4}{\partial y} = -\frac{16\sigma^t}{3k_t}(T^3\frac{\partial T}{\partial y}). \tag{1}$$

Accounting for the adherence between the solid boundaries and the flowing fluid, we have the velocity slip (U_{slip}) and temperature jump (T_{slip}).

$$T_{slip} = \frac{2-\sigma_e}{\sigma_e}\frac{\lambda r}{Kn}\left(\frac{2r}{r+1}\right)\frac{\partial T}{\partial y} + \left[\frac{2-\sigma_e}{\sigma_e}\frac{\lambda r}{Kn}\left(\frac{2r}{r+1}\right)\right]^2 \frac{\sigma_e}{4r}\frac{(r+1)Pr}{(2-\sigma_e)}\frac{\partial^2 T}{\partial y^2}, \tag{2}$$

$$U_{slip} = \frac{\mu}{\rho}[\frac{2}{3}(\frac{3-\sigma_m J^2}{\sigma_m} - \frac{3}{2}\frac{1-J^2}{Kn})\lambda r\frac{\partial u}{\partial y} - (J^4 + \frac{2}{Kn^2}(1-J^2))\lambda r^2\frac{\partial^2 u}{\partial y^2}], \tag{3}$$

$$T_{slip} = b_1\frac{\partial T}{\partial y} + b_2\frac{\partial^2 T}{\partial y^2}, \qquad U_{slip} = \frac{\mu}{\rho}[a_1\frac{\partial u}{\partial y} - a_2\frac{\partial^2 u}{\partial y^2}], \tag{4}$$

Subjected to the assumptions above, the momentum, energy continuity, and concentration equations of Williamson-Casson dissipative fluid are given by;

$$\frac{\partial u}{\partial x} + \frac{\partial v}{\partial y} = 0, \tag{5}$$

$$u\frac{\partial u}{\partial x} + v\frac{\partial u}{\partial y} = \frac{\mu}{\rho}\left(1+\frac{1}{\beta_1}\right)\frac{\partial^2 u}{\partial y^2} + \sqrt{2}\Gamma_0\frac{\mu}{\rho_f}\left(\frac{\partial u}{\partial y}\right)\frac{\partial^2 u}{\partial y^2} - \frac{\sigma^*(T)B(x)^2}{\rho}u - \frac{g\cos(\alpha)}{\rho}\left[\Xi(T)+\Xi(C)\right], \tag{6}$$

$$u\frac{\partial T}{\partial x} + v\frac{\partial T}{\partial y} + \frac{1}{\rho c_p}\frac{\partial q_r}{\partial y} - \frac{\sigma^*(T)B(x)^2}{\rho C_p}u^2 + Q_p = \frac{1}{\rho C_p}\frac{\partial^2 T}{\partial y^2} + \frac{\mu}{\rho C_p}\left(\frac{\partial u}{\partial y}\right)^2\left[\left(1+\frac{1}{\beta_1}\right) + \sqrt{2}\Gamma_0\frac{\partial u}{\partial y}\right], \tag{7}$$

$$u\frac{\partial C}{\partial x} + v\frac{\partial C}{\partial y} = Dq\frac{\partial^2 C}{\partial y^2} + \frac{D_T}{T_\infty}\frac{\partial^2 T}{\partial y^2}, \tag{8}$$

Where

$$Q_p = h_i\left[u^2\frac{\partial^2 T}{\partial x^2} + 2uv\frac{\partial^2 T}{\partial y \partial x} + v\frac{\partial u}{\partial y}\frac{\partial T}{\partial x} + v^2\frac{\partial^2 T}{\partial y^2} + u\frac{\partial v}{\partial x}\frac{\partial T}{\partial y} + v\frac{\partial v}{\partial y}\frac{\partial T}{\partial y} + u\frac{\partial u}{\partial x}\frac{\partial T}{\partial x}\right], \tag{9}$$

Subject to the second order slip and temperature jump conditions (Titiloye et al. 2021):

$$u = U_w(x) + U_{slip},\ v = 0,\ T = T_w + T_{slip},\ C = C_w, at\ \ y = A(x+c)^{\frac{1-m}{2}},$$
$$u = 0,\ \ T = T_\infty,\ \ C = C_\infty \ \ as \ \ y \to \infty. \tag{10}$$

Where u and v denotes the velocity along x and y - axis respectively, h_i is the relaxation constant, ν is the viscosity, β is the Casson, σ signifies electrical conductivity, B_0 signifies magnetic constant, ρ signifies density, T_∞ signifies the temperature at the free stream, T signifies temperature, α is the incline angle, κ signifies thermal conductivity, Γ_0 is the Williamson time constant c_p signifies heat capacity, D_q signifies mass diffusivity, C signifies concentration, D_T signifies thermophoretic diffusion coefficient, μ signifies coefficient of viscosity, q_r signifies radiative heat flux, b_1, b_2 and a_1, a_2 signifies slip terms respectively.

Implementing the similarity variables below, Akolade et al. 2021a, Idowu et al. 2020;

$$\psi = \left(\frac{2\nu d_0 x^{m+1}}{m+1}\right)^{\frac{1}{2}} F(\tau), v = -\frac{\partial \psi}{\partial x}, u = \frac{\partial \psi}{\partial y}, \theta(\tau) = \frac{T - T_\infty}{T_w - T_\infty}, \phi(\tau) = \frac{C - C_\infty}{C_w - C_\infty}, \tau = \left(\frac{(m+1)d_0 x^{m-1}}{2\nu}\right)^{\frac{1}{2}} y. \tag{11}$$

Applying equation (5) on equations (6) - (10), the resulting ODE systems becomes;

$$\left\{\left(1 + \frac{1}{\beta_1}\right) + \beta_2 F''\right\} F''' + FF'' - \left(\frac{2}{m+1}\right)\left[m\left(F'\right)^2 + \frac{Ha^2}{(1+\xi_2\theta)} F' - \cos(\alpha)\left[G_t(\theta + \xi_1\theta^2) + G_c(\phi + \xi_3\phi^2)\right]\right] = 0, \tag{12}$$

$$\left(1 + \frac{4Nr}{3}\right)\theta'' - Pr\ \Omega\left(\frac{m+1}{2}\theta'' F^2 - \frac{m-3}{2}\theta' FF'\right) + Pr\ F\ \theta' +$$
$$Ec\ Pr\left(\frac{2}{m+1}\right)\frac{Ha^2}{(1+\xi_2\theta)}(F')^2 + Ec\ Pr\left\{\left(1 + \frac{1}{\beta_1}\right) + \beta_2 F''\right\}\left(F''\right)^2 = 0, \tag{13}$$

$$\phi'' + Sc\ F\ \phi' + Sr\ \theta'' = 0, \tag{14}$$

Subjected to:

$$F'(\tau) = 1 + \Lambda_1 F''(\tau) - \Lambda_2 F'''(\tau),\ \theta(\tau) = 1 + \Lambda_3\theta'(\tau) + \Lambda_4\theta''(\tau),$$
$$F(\tau) = \left(\frac{1-m}{1+m}\right)\chi\left[F'(\tau)\right],\ \phi(\tau) = 1,\ at\ \tau = \chi,$$
$$F'(\tau) = 0,\ \ \theta(\tau) = 0,\ \ \phi(\tau) = 0, \qquad as \quad \tau \to \infty. \tag{15}$$

Where $\chi = A\sqrt{\frac{m+1}{2\nu}d_0}$, $\Lambda_1 = \frac{S_1}{\sqrt{Re_x^{-1}}}$, $\Lambda_2 = \frac{S_2}{Re_x^{-1}}$, $\Lambda_3 = \frac{S_3}{\sqrt{Re_x^{-1}}}$, $\Lambda_4 = \frac{S_4}{Re_x^{-1}}$, $= \frac{\grave{o}_1}{Re_x}$,

$S_1 = a_1\nu\left(\frac{(m+1)}{2}\right)^{\frac{1}{2}}$, $S_2 = a_2\nu\left(\frac{(m+1)}{2}\right)$, $S_3 = b_1\nu\left(\frac{(m+1)}{2}\right)^{\frac{1}{2}}$, $S_4 = b_2\nu\left(\frac{(m+1)}{2}\right)$, $Gr = \frac{\beta_1 g(T_w - T_\infty)}{d_0\nu U_0}$,

$Gc = \frac{\beta_3 g(C_w - C_\infty)}{d_0\nu U_0}$, $\xi_1 = \frac{\beta_2}{\beta_1}(T_w - T_\infty)$, $Pr = \frac{\mu Cp}{k^*}$, $\beta_2 = \frac{\Gamma_0 U_0 d_0^3 x^{3m-1}}{\sqrt{2\nu}}$, $Nr = \frac{4\sigma^t T_\infty^3}{k_t k^*}$, $Pr = \frac{c_p\mu}{k^*}$,

$\xi_2 = \xi_0(T_w - T_\infty)$, $\xi_3 = \frac{\beta_4}{\beta_3}(C_w - C_\infty)$, $Ha = B_0\left(\frac{\sigma}{\rho d_0}\right)^{\frac{1}{2}}$, $\Omega = d_0 h_i$, $Sr = \frac{D_T}{T_\infty}\frac{T_w - T_\infty}{C_w - C_\infty}$, $Sc = \frac{\nu}{Dq}$,

.

Ω represent the dimensionless thermal relaxation, Gc Grashof number for concentration, Gr Grashof number for temperature, Ec Eckert number, Ha dimensionless magnetic field parameter, ξ_1 nonlinear thermal expansion coefficient, ξ_3 nonlinear concentration expansion coefficient, Pr Prandtl number, Sc Schmidt number, Sr Soret number, β_1 Casson parameter, β_2 Williamson parameter, Nr Radiation parameter, and $S_{1,2}$, $\Lambda_{1,2,3,4}$ are slip and jump factors.

Equations (12) - (15) are in the domain $[\chi,\infty)$. To ease the computation, the least similarity variable $\eta = A\left(\frac{(m+1)d_0}{2\nu}\right)^{\frac{1}{2}}$ is assumed, then set $f(\eta) = f(\tau-\chi) = F(\tau)$, $g(\eta) = g(\tau-\chi) = \theta(\tau)$, $h(\eta) = h(\tau-\chi) = \phi(\tau)$ then, the flow domain along with the corresponding governing systems becomes, $[0,\infty)$;

$$\left\{\left(1+\frac{1}{\beta_1}\right)+\beta_2 f''\right\} f''' + ff'' - \left(\frac{2}{m+1}\right)\left[m\left(f'\right)^2 + \frac{Ha^2}{(1+\xi_2 g)} f' - \cos(\alpha)\left[G_t(g+\xi_1 g^2)+G_c(h+\xi_3 h^2)\right]\right] = 0, \tag{16}$$

$$\left(1+\frac{4Nr}{3}\right)g'' - Pr\,\Omega\left(\frac{m+1}{2} g'' f^2 - \frac{m-3}{2} g' f f'\right) + Pr\; f\; g' + Ec\,Pr\left(\frac{2}{m+1}\right)\frac{Ha^2}{(1+\xi_2 g)}(f')^2 + Ec\,Pr\left\{\left(1+\frac{1}{\beta_1}\right)+\beta_2 f''\right\}(f'')^2 = 0, \tag{17}$$

$$h'' + Sc\; f\; h' + Sr\; g'' = 0, \tag{18}$$

$$f'(\eta) = 1+\Lambda_1 f''(\eta) - \Lambda_2 f'''(\eta),\; g(\eta) = 1+\Lambda_3 g'(\eta) + \Lambda_4 g''(\eta),$$

$$f(\eta) = \left(\frac{1-m}{1+m}\right)\chi\left[f'(\eta)\right],\; h(\eta) = 1,\; at\;\; \eta = 0,$$

Subjected to: $f'(\eta) = 0,\;\; g(\eta) = 0,\;\; h(\eta) = 0, \qquad as \;\;\; \eta \to \infty.$ (19)

The flow characteristics namely the Skin friction, Nusselt number, and the Sherwood number are given as thus;

$$Re_x^{\frac{1}{2}} C_{f_x} = 2\sqrt{\frac{m+1}{2}} f''(0)\left[\left(1+\frac{1}{\beta_1}\right)+\frac{\beta_2}{2}(f''(0))\right], \tag{20}$$

$$Re_x^{-\frac{1}{2}} Nu_x = -(1+\frac{4}{3}Nr)g'(0), \tag{21}$$

$$Re_x^{-\frac{1}{2}} Sh_x = -h'(0). \tag{22}$$

Method of Solution

To establish the approximate solution of the governing ODEs in equation (16) - (19) which the closed form solution is far easily obtained, we employed the collocation technique with Legendre polynomial basis function, for detail see Oyekunle *et al*. 2021; Akolade et al. 2022.

Implementation of Legendre-based Collocation Method

The assumed trial functions $F_1(\eta), F_2(\eta), \Theta(\eta)\; and\; \Phi(\eta)$ are assumed as the sum of Legendre base functions

$$f(\eta) = \sum_{n=0}^{N} a_n W_n\left(\frac{2\eta}{L}-1\right),\quad g(\eta) = \sum_{n=0}^{N} b_n W_n\left(\frac{2\eta}{L}-1\right),\; h(\eta) = \sum_{n=0}^{N} c_n W_n\left(\frac{2\eta}{L}-1\right), \tag{23}$$

where a_n, b_n, and c_n are the constants to be determined. Equation (23) is substituted into the boundary conditions in equation (19) to give;

$$\left[\frac{d}{d\eta}\sum_{n=0}^{N} a_n W_n\left(\frac{2\eta}{L}-1\right) - \Lambda_1 \frac{d^2}{d\eta^2}\sum_{n=0}^{N} a_n W_n\left(\frac{2\eta}{L}-1\right) + \Lambda_2 \frac{d^3}{d\eta^3}\sum_{n=0}^{N} a_n W_n\left(\frac{2\eta}{L}-1\right)\right]_{\eta=0} = 1 \tag{24}$$

$$\left[\sum_{n=0}^{N} b_n W_n\left(\frac{2\eta}{L}-1\right) - \Lambda_3 \frac{d}{d\eta}\sum_{n=0}^{N} b_n W_n\left(\frac{2\eta}{L}-1\right) - \Lambda_4 \frac{d^2}{d\eta^2}\sum_{n=0}^{N} b_n W_n\left(\frac{2\eta}{L}-1\right)\right]_{\eta=0} = 1, \tag{25}$$

$$\left[\sum_{n=0}^{N} a_n W_n\left(\frac{2\eta}{L}-1\right) - \left(\frac{1-m}{1+m}\right)\chi\left(\frac{d}{d\eta}\sum_{n=0}^{N} a_n W_n\left(\frac{2\eta}{L}-1\right)\right)\right]_{\eta=0} = 0,\; \left[\sum_{n=0}^{N} c_n W_n\left(\frac{2\eta}{L}-1\right)\right]_{\eta=0} = 1, \tag{26}$$

$$\left[\frac{d}{d\eta}\sum_{n=0}^{N}a_nW_n\left(\frac{2\eta}{L}-1\right)\right]_{\eta=L}=0,\quad\left[\sum_{n=0}^{N}b_nW_n\left(\frac{2\eta}{L}-1\right)\right]_{\eta=L}=0,\quad\left[\sum_{n=0}^{N}c_nW_n\left(2\eta-1\right)\right]_{\eta=L}=0. \tag{27}$$

Substituting equations (23) into equations $(12)-(15)$, residues $R_f(\eta,a_n,b_n,c_n),\quad R_{g_2}(\eta,a_n,b_n,c_n$, and $R_h(\eta,a_n,b_n,c_n)$ are derived.

With the following steps the residues are minimized closed to zero;

$$\text{for } \delta\left(\eta-\eta_j\right)=\begin{cases}1, & \eta=\eta_j\\ 0, & otherwise,\end{cases} \tag{28}$$

$$\int_0^L R_h\delta\left(\eta-\eta_j\right)d\eta=R_h\left(\eta_j,a_n,b_n,c_n\right)=0,\quad for\ j=1,2,..N-1,$$

$$\int_0^L R_f\delta\left(\eta-\eta_j\right)d\eta=R_f\left(\eta_j,a_n,b_n,c_n\right)=0,\quad for\ j=1,2,..N-2$$

$$\int_0^L R_g\delta\left(\eta-\eta_j\right)d\eta=R_g\left(\eta_j,a_n,b_n,c_n\right)=0,\quad for\ j=1,2,..N-1, \tag{29}$$

$$\eta_j=\frac{1}{2}\left(1-cos\left(\frac{j\pi}{N}\right)\right)$$

Where is the shifted Gauss-Lobatto points?

In this procedure, 3N by 3 unknown coefficients with 3N+3 algebraic equations with 3N+3 algebraic equations are obtained. With the help of the MATHEMATICA symbolic package, a collocation is set and NSolve is used to obtain the roots.

$$collocationpoints=NSolve\left[Expand\left[LegendreW\left[N-1,\quad 2\frac{\eta}{L}-1\right]\right]=0,\eta\right] \tag{30}$$

Results and Discussion

The flow, energy, and concentration profiles for distinct behavior of the distribution parameters are profiled and discussed. For the record, the following parameters are maintained constant throughout the computation else otherwise stated $Ha=Gr=Gc=1.0$, $\xi_1=\xi_3=0.5$, $\xi_2=0.2$, $h_2=0.5$, $h_4=0.2$, $h_1=0.2$, $h_3=0.2$, $\xi_4=0.1$, $Ec=0.1$, $Sr=0.3$. Momentum, temperature, concentration, skin-friction, Nusset number, and Sherwood number behavior, performance, and characterization on the Williamson-Casson fluid flow through an inclined geometry is presented in this section. The record in Table 1 elucidates the performance of the Legendre-based collocation method with the earlier studies of Devi and Prakash (2016), and Sharma and Shaw (2022), evidently, the results herein are in good agreement with the works in the literature. Graphically Figures 2 - 9 highlight the impacts of the flow pertinent parameters on the flow, energy, concentration, and characteristics profiles.

Figure 2 unavailing the action of the imposed Lorentz force acting against the flow surface indicated that higher magnetization drag down the flow field but positively enhanced the temperature of the fluid and concentration. Due to a reduction in fluid momentum force pictured in figure 2(a-c), a rise in Ha further identified that Williamson fluid conduct lower heat energy and is easily dragged down but maintains higher concentration than the Casson fluid. The impacts of the modified heat flux (Ω), also called non-Fourier's law (Cattaneo-Christov) are presented in figure 3. Figure 3(a) enumerated the little impact of relaxation time on the velocity field on the wall and figure 3(b) clarifies its significant influence on the temperature field. A reduction in the fluid temperature is experienced in the entire flow domain, thus indicating more time will be needed for successful heat transport in the considered geometry. Meanwhile, Williamson fluid shows a faster temperature reduction than the Casson fluid in the flow medium, but a contrary effect is seen on the fluid flow surface. This is attributed to the non-newtonian fluid chemical properties of the two fluids.

Soret (thermal-diffusion) being the mass fluxes generated by the heat energy gradient is seen accelerating the fluid momentum, and concentration significantly as the parameter Sr increases. The impact gave little effect on the temperature profiles. Concurrently, figure 5 profiled an increasing behavior to a higher magnitude of radiation number (Nr). The behavior indicated that both fluids gave the accelerating behavior. This result on the profile $g(\eta)$ is not far-fetched since Nr is radiative heat energy, thus, the energy profile is set to magnify for a rising Nr. Response of the internally generated heat on the velocity, temperature, and concentration distributions for both non-Newtonian fluids are showcased in figure 6. Mathematically, Ec represent the ratio of the change in enthalpy difference. The heat generated tend to reduce both fluid momentum and concentration close to the boundary surface, but energized all three profiles positively at the boundary layer region (see Figure 6 a-c).

The behavior of the thermal Grashof coefficient (Gr) and solutal Grashof coefficient (Gc) on the velocity, temperature, and concentration distributions are enumerated in figures 7(a-c) and 8(a-c) respectively. These terms (Gr,Gc) are characterized by the temperature and concentration variation difference due to the buoyancy effect. A rise in corresponding fluid flow of both Casson and Williamson fluid for greater values of Gr and Gc is profiled in figures 7(a) and 8(a) respectively. However, a corresponding decrease in concentration distribution is

recorded in Figures 7(c) and 8(c) accordingly as Gr and Gc upsurge. On the other hand, energy transfer of both Casson and Williamson fluid resulted in an opposite characterization as seen in Figures 7(b) and 8(b). Therein, a rise of Gr and Gc increases the temperature of Casson fluid but diminished the temperature of Williamson fluid. Physically, this result may be attributed to the lower heat enhancement of Williamson fluid compared to the Casson fluid.

Moreover, the fluid flow and heat transfer engineering of interest is depicted in figure 9 for both impact of the material relaxation time Ω and the magnetic field effect Ha. Figure 9(a) elucidates that the skin friction increases as Ha grows, and skin friction decreases as the time relaxation number grows. On the same note, the Nusset number (heat transfer coefficient) decreases as the time relaxation number and the Hartman number magnifies.

Conclusion

So far, the impact of soret, modified hat flux, magnetization, convection, dissipation, and radiation have been enumerated in the comparative and numerical investigation of Williamson-Casson fluid flow over an inclined slendering surface. The study adopted a well-posed similarity variable to convert the governing systems of PDEs into ODE equations and then solved numerically via the novel Legendre-based collocation method. The provided table authenticates the performance of the imposed method. The following conclusions were drawn:

- The magnetization effect (Ha) slows down the momentum but energized the temperate and the solutal field.
- The relaxation parameter signified that more time will be needed for successive heat transfer in both fluid models, thus reducing the flow velocity of the wall surface.
- Williamson fluid possessed lower heat enhancement compared to the Casson fluid.
- The Soret mechanism promotes the velocity, temperature, and concentration fields.
- Radiation numbers upsurge the temperature field significantly.
- A rise in Ha decreased the Nusset number, but magnified the skin friction.

Table 1: Comparison of results of Skin friction coefficient heat transfer rate.

Value $-f''(0)$				Value $-g'(0)$ such that $\Lambda_1 = \chi = 0$		
Λ_1	χ	Devi & Prakash (2016)	Present work	Pr	Sharma & Shaw (2022)	Present work
0.0	0.2	0.9248281	0.924821298	0.2	0.16631332	0.17003133
0.2	0.25	0.7333949	0.733385610	0.7	0.45540012	0.45391747
0.2	0.3	–	0.738594316	2.0	0.91102381	0.91135768
0.2	0.5	0.7595701	0.759562561	7.0	1.89432002	1.89431426
0.5	0.5	–	0.578436131	20	3.35045413	3.35065976
0.5	0.6	–	0.584199971	70	6.46010020	6.46011132

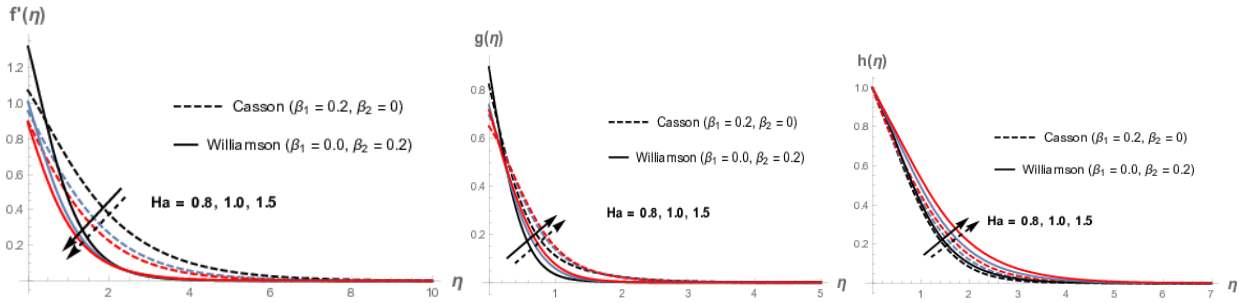

(a) (b) (c)

Figure 2: Impact of magnetization on (a) $f'(\eta)$, (b) $g(\eta)$, and (c) $h(\eta)$.

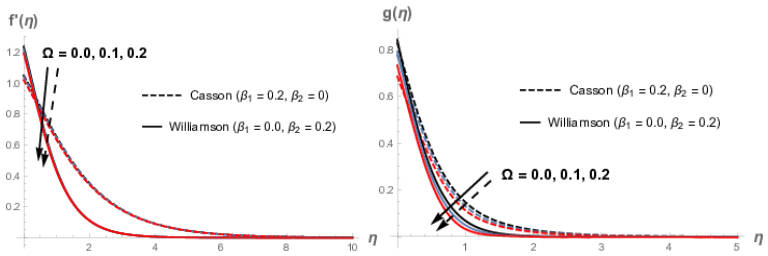

(a) (b)

Figure 3: Impact of Relaxation time on (a) $f'(\eta)$, and (b) $g(\eta)$.

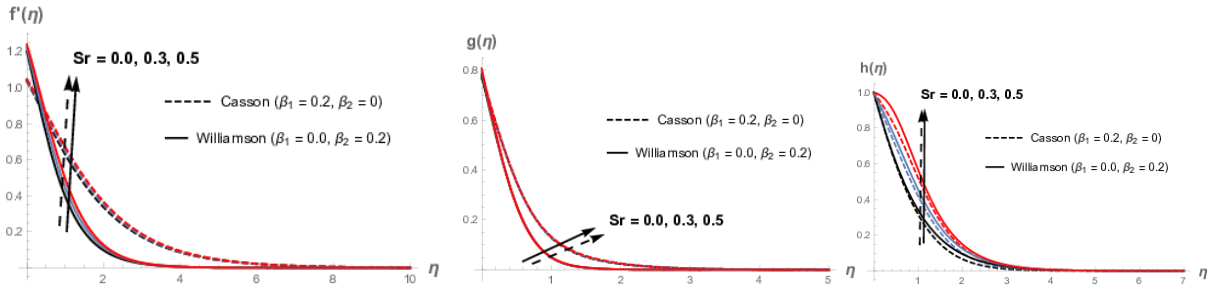

(a) (b) (c)

Figure 4: Impact of Soret number on (a) $f'(\eta)$, (b) $g(\eta)$, and (c) $h(\eta)$.

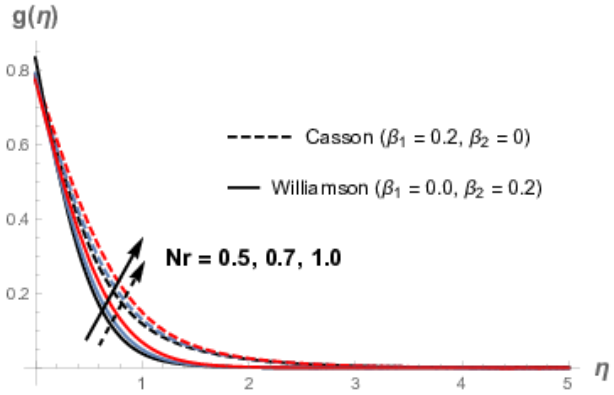

Figure 5: Impact of Radiation on (a) $g(\eta)$.

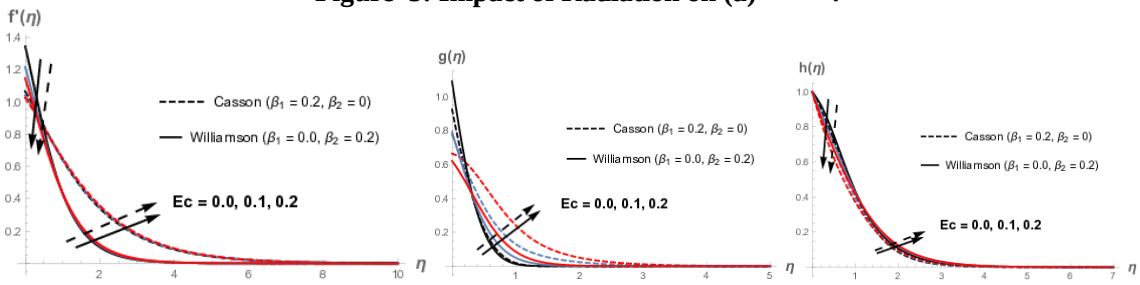

(a) (b) (c)

Figure 6: Impact of Eckert number on (a) $f'(\eta)$, (b) $g(\eta)$, and (c) $h(\eta)$.

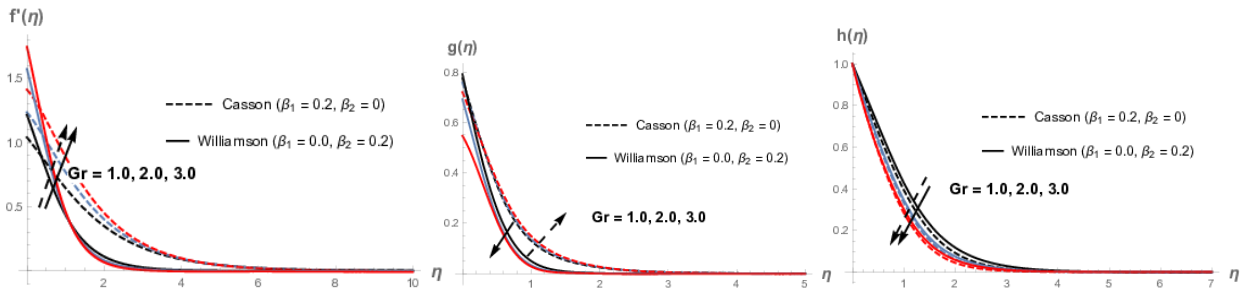

(a) (b) (c)

Figure 7: Impact of thermal convection number on (a) $f'(\eta)$, (b) $g(\eta)$, and (c) $h(\eta)$.

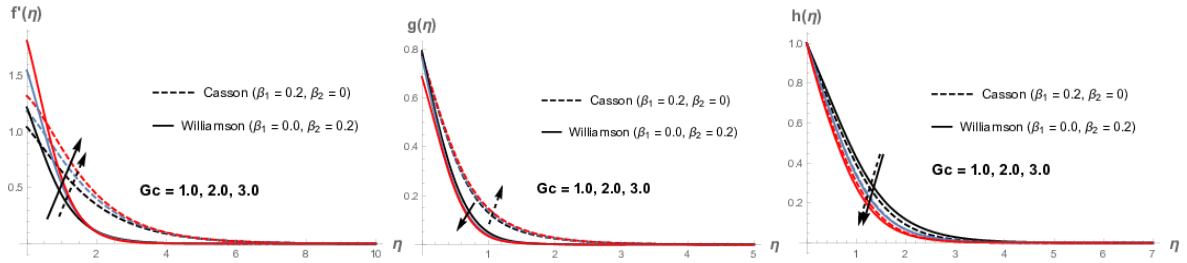

(a) (b) (c)

Figure 8: Impact of solutal convection number on (a) $f'(\eta)$, (b) $g(\eta)$, and (c) $h(\eta)$.

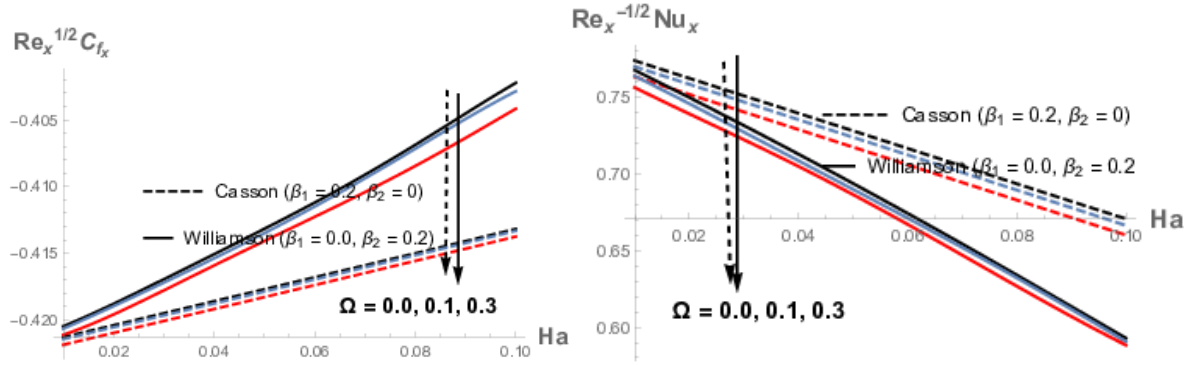

(a) (b)

Figure 9: Impact of some flow parameters on (a) Skin friction, and (b) Nusset number.

References

Akolade M. T., Tijani, Y. O. (2021). A comparative study of threedimensional flow of Casson–Williamson nanofluids past a riga plate: Spectral quasi-linearization approach. Partial Differential Equations in Applied Mathematics. 4, 1-12. 100108.

Akolade MT, Idowu AS, Adeosun AT. (2021a) Multislip and Soret-Dufour influence on nonlinear convection flow of MHD dissipative casson fluid over a slendering stretching sheet with generalized heat flux phenomenon. Heat Transfer. 2021;1–21.

Akolade M.T., Adeosun A.T., Olabode J.O. (2021b) Influence of Thermophysical Features on MHD Squeezed Flow of Dissipative Casson Fluid with Chemical and Radiative Effects, J. Appl. Comput. Mech., 7(4), 2021, 1999–2009.

Akolade MT, Oyekunle TL, Momoh HO, Awad MM. (2022) Thermophoretic movement, heat source, and sink influence on the Williamson fluid past a Riga surface with positive and negative Soret-Dufour mechanism. Heat Transfer. 2022; 1-19.

Bhuvaneswari, M., Sivasankaran, S., Niranjan, H., Eswaramoorthi, S. (2019). Cross Diffusion Effects on MHD Convection of Casson-Williamson Fluid over a Stretching Surface with Radiation and Chemical Reaction. In: Rushi Kumar, B., Sivaraj, R., Prasad, B., Nalliah, M., Reddy, A. (eds) Applied Mathematics and Scientific Computing. Trends in Mathematics. Birkhäuser, Cham. https://doi.org/10.1007/978-3-030-01123-9_15

Cattaneo C. (1948) Sulla conduzione del calore, AttiSemin. Mat Fis Univ Modena Reggio Emilia. 3:83-101.

Christov CI. (2009) On frame indifferent formulation of the Maxwell-Cattaneo model of finite-speed heat conduction. Mech Res Comm. 36:481-486.

Devi, S. P. A., Prakash, M., (2016) Slip Flow Effects over Hydromagnetic Forced Convective Flow over a Slendering Stretching Sheet Journal of Applied Fluid Mechanics , Vol. 9, No. 2, pp. 683-692.

Fourier JBJ. (1822) Thorie Analytique De La Chaleur, Paris.

Hayat, T., Farooq, M., Alsaedi, A., Al-Solamy F., (2015). Impact of Cattaneo-Christov heat flux in the flow over a stretching sheet with variable thickness. AIP Advances 5, 087159.

Idowu A.S., Akolade M.T., Oyekunle T.L., and Abubakar J.U. (2021) Nonlinear convection flow of dissipative Casson nanofluid through an inclined annular microchannel with a porous medium. Heat Trans. Res., 50(4): 3388-3406.

Idowu AS, Akolade MT, Abubakar JU, Falodun BO. (2020) MHD free convective heat and mass transfer flow of dissipative Casson fluid with variable viscosity and thermal conductivity effects. J Taibah Uni Sci. 14(1):851-862.

Kumar, K.A., Sugunamma, V., Sandeep, N. (2019) MHD stagnation point flow of Williamson and Casson fluids past an extended cylinder: a new heat flux model. SN Appl. Sci. 1, 705.

Marin E. (2011). Does Fourier's law of heat conduction contradict the theory of relativity. Latin Am J Phys Educ. 5(2):402-405.

Oke, A. S., Mutuku, W. N., Kimathi, M., Animasaun, I. L., (2021). Coriolis effects on MHD newtonian flow over a rotating non-uniform surface. Proc IMechE Part C: J

Mechanical Engineering Science. Vol. 235(19) 3875–3887.

Olabode J. O., Idowu, A. S., Akolade M. T., Titiloye, E. O., (2021). Unsteady flow analysis of Maxwell fluid with temperature dependent variable properties and quadratic thermo-solutal convection influence. Partial Differential Equations in Applied Mathematics. 4 (2021) 100078, 1-12

Oyekunle, Timothy L.; Akolade, Mojeed T.; and Agunbiade, Samson A., (2021). Thermal-Diffusion and Diffusion-Thermo Effects on Heat and Mass Transfer in Chemically Reacting MHD Casson Nanofluid with Viscous Dissipation, Applications and Applied Mathematics: An International Journal (AAM), Vol. 16, Iss. 1, Article 39.

Sarkar, T., Reza-E-Rabbi, S., Arifuzzaman, S.M., Ahmed, R., Khan, M.S., Ahmmed, S.F. (2019). MHD radiative flow of Casson and Williamson nanofluids over an inclined cylindrical surface with chemical reaction effects. International Journal of Heat and Technology, Vol. 37, No. 4, pp. 1117-1126. https://doi.org/10.18280/ijht.370421.

Sharma R.P., Shaw S., (2022). MHD Non-Newtonian Fluid Flow past a Stretching Sheet under the Influence of Non-linear Radiation and Viscous Dissipation, J. Appl. Comput. Mech., 8(3), 2022, 949–961.

Sivanandam, S., Eswaramoorthi, S. (2022). Entropy optimization of MHD Casson-Williamson fluid flow over a convectively heated stretchy sheet with Cattaneo-Christov dual flux. Scientia Iranica, (), -. doi: 10.24200/sci.2022.58291.5654

Titiloye E. O., Adeosun, A. T., Gbadeyan, J. A., (2021). Influence of Chemical Reaction and Arrhenius Activation Energy on Hydromagnetic Non-Darcian Casson Nanofluid Flow with Second-Order Slip Condition. International Journal of Engineering Research in Africa. Vol. 54, pp 100-117.

Upadhya S. M., Raju C.S.K., Saleem S., Alderremy A.A., Mahesha, (2018). Modified Fourier heat flux on MHD flow over stretched cylinder filled with dust, Graphene and silver nanoparticles. Results in Physics Volume 9, Pages 1377-1385.

Vishalakshi AB, Mahabaleshwar US, Sarris IE. (2022). An MHD Fluid Flow over a Porous Stretching/Shrinking Sheet with Slips and Mass Transpiration. Micromachines (Basel). 12;13(1):116. doi: 10.3390/mi13010116. PMID: 35056281; PMCID: PMC8780972.